

On the modelling of an aluminium alloy milling: 3D FEM approach

M. Asad*, T. Mabrouki**

*Center of excellence in science and applied technologies, Islamabad, Pakistan, E-mail: masadakhtar@yahoo.com

**Université de Lyon, INSA-Lyon, LaMCoS, UMR5259, F69621, France, E-mail: tarek.mabrouki@insa-lyon.fr

crossref <http://dx.doi.org/10.5755/j01.mech.19.5.5538>

1. Introduction

Finite element (FE) modelling of machining processes had proved its effectiveness in unveiling multiphysical phenomena occurring at tool workpiece interface. These models are worthy in improving the production efficiency in terms of cutting tool geometry and optimal cutting parameters selection. FE-models are equally valuable in selecting and improving existing machine tools in aspect of their dynamic stability characteristics, to minimize the cutting vibrations [1]. Precious efforts had been started since 1970s to model the cutting process by FE methods. Initially, temperature fields in the chip and cutting tool were investigated [2]. Since then, valuable researches focusing various aspects of machining have been conducted and an exhaustive literature is now available. Nevertheless, complex nature of actual cutting phenomena and time consuming computing numerical techniques had restricted the researchers to limit their models to simplified 2D approaches with plane strain hypothesis. Later, assumption holds good for: depth of cut $a_p \gg$ cutting feed (f) i.e. rough machining case. Whilst this hypothesis does not work well for: $a_p \approx f$ i.e. for semi-finish and finish machining cases.

Under the foresaid machining cases, 3D models become inevitable to get the factual physical apprehension of ongoing processes. 3D models are also essential to realize some interesting features of cutting phenomena e.g. oblique machining [3], 3D cutting tool wear prediction [4] etc. Which otherwise are difficult to comprehend with 2D models.

In this framework, the present contribution put forwards a 3D FE approach to perform a parametric study highlighting the effects of depth of cut and cutting speed on surface and chip morphologies, for machining an aerospace grade aluminium alloy A2024-T351. Explicit approach of a FE code ABAQUS® (version 6.9.1) have been exploited to model the rough to finish machining operations for down cut milling. Numerical modelling and simulation work has been conceived in two successive steps. Primarily, a 3D model for rough down cut milling case, based on authors previously developed 2D model [5] was established. To validate the model, numerical results concerning chip morphology and cutting force were compared with the experimental data. Afterwards, numerical parametric study on the effects of lower a_p values i.e. of the order of f (semi-finish and finish machining cases) and cutting speeds, on surface finish and chip morphology was conducted.

2. Three-dimensional FE model for orthogonal milling

2.1. Geometry, meshing and boundary conditions

In the present section the conceived geometry, boundary conditions, meshing, interactions and hypothesis to build a FE based 3D down-cut peripheral milling case are discussed. During the machining operation, cutting tool and workpiece come in contact. Numerically difficult to build contact and interaction definitions need special attention in developing FE based cutting models. To overcome contact complexities, the workpiece was modelled in three parts; chip, cutter path and machined part (Fig. 1). Tie-constraint algorithm (ABAQUS® built in algorithm) was used to assemble these parts. Once assembled, these parts behaved as a single entity “workpiece” and not as individual parts. Workpiece was meshed with thermally coupled continuum brick elements C3D8RT, to run coupled temperature-displacement calculations.

Literature study shows that whatever is the type of elements, mesh density plays a vital role to get physical results from FE based analyses. Unfortunately in the literature dealing with FE based cutting models, there is no defined criterion for an optimized mesh density. Mostly, very fine mesh (2-20 μm) for complex plasticity problems is used. However, time penalty is quiet high for very fine meshes. Recently, Asad [6] in his doctoral work has performed a mesh sensitivity test for six different mesh densities for a 2D orthogonal cutting model and found an optimal mesh density for $27 \times 27 \mu\text{m}$ for the studied material. In the present work a mesh density of $28 \times 28 \times 40 \mu\text{m}$ decreasing to $21 \times 28 \times 40 \mu\text{m}$ has been conceived in the variable section of chip for down cut milling model. The cutting tool was assumed as a rigid body and was meshed with bilinear rigid quadrilateral elements R3D4.

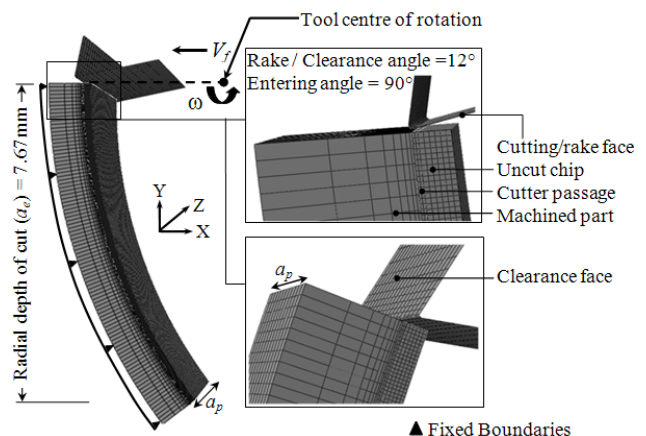


Fig. 1 3D geometrical model for down cut milling

Schematic representation of the conceived model, for 90° entering angle and 0° edge inclination angle is shown in Fig. 1. During the simulation, tool cutting edge was simultaneously orthogonal to the cutting and the feed velocities. This represents a three dimensional orthogonal cutting case.

Further, it can be seen in the figure that the workpiece is constrained with fixed boundary conditions. While tool can advance with feed velocity V_f (feed rate $f=0.2$ mm/tooth) in the negative X -axis direction and can rotate with angular velocity ω in the anticlockwise direction, simultaneously. A 25 mm diameter milling tool with two cutters was used in the present work. As the tool rotates and advances simultaneously, the cutter traces trochoidal path. This produces variable section chip with decreasing uncut chip thickness. To avoid the big efforts involved at lower uncut chip thickness values (with very fine mesh density), present model represents a 3D milling model with a radial depth of cut $a_e = 7.67$ mm. This represents an uncut chip thickness (UCT) up to 160 μm . The trochoidal path equations were used to model milling cutter path zone (cutter path/chip separation zone) and chip section geometry.

The conceived 3D cutting model employs well known Zorev's stick-slip friction model to define the frictional interaction between the chip and tool with an average friction coefficient $\mu = 0.17$.

2.2. Material behaviour and chip separation model

Constitutive material modelling equations are the same as used in authors recent research work [7]. However, some necessary details are mentioned in the present paper. Jhonson and Cook (JC) equivalent stress model is employed in the model as presented by following expression:

$$\bar{\sigma}_{JC} = (A + B\bar{\epsilon}^n) \left[1 + C \ln \left[\frac{\dot{\bar{\epsilon}}}{\dot{\bar{\epsilon}}_0} \right] \right] \left[1 - \left[\frac{T - T_r}{T_m - T_r} \right]^m \right]. \quad (1)$$

While, JC shear failure model is used as a damage initiation criterion, as represented by following relation:

$$\bar{\epsilon}_{0i} = \left[D_1 + D_2 \exp \left[D_3 \frac{P}{\bar{\sigma}} \right] \right] \left[1 + D_4 \ln \left[\frac{\dot{\bar{\epsilon}}}{\dot{\bar{\epsilon}}_0} \right] \right] \times \left[1 + D_5 \left[\frac{T - T_r}{T_m - T_r} \right] \right], \quad (2)$$

where, A is the initial yield stress, B is the hardening modulus, C is the strain rate dependency coefficient, m is the thermal softening coefficient, n is the work-hardening exponent, T is the temperature at a given calculation instant, T_r is the room temperature, T_m is the melting temperature, $\bar{\epsilon}$ is the equivalent plastic strain, $\dot{\bar{\epsilon}}$ is the plastic strain rate and $\dot{\bar{\epsilon}}_0$ is the reference strain rate. D_1 to D_5 are the coefficients of JC material shear failure initiation criterion, p is the hydrostatic pressure, $\bar{\sigma}$ is the von Mises equivalent stress and $p/\bar{\sigma}$ is the stress triaxiality.

Damage is initiated when the scalar damage parameter ω_{0i} exceeds 1, based on Eq. (3):

$$\omega_{0i} = \sum \frac{\Delta \bar{\epsilon}}{\bar{\epsilon}_{0i}}. \quad (3)$$

Whereas, damage evolution parameter can be defined in the form a scalar stiffness degradation parameter D that can evolve linearly (Eq. (4)), used for cutter path section or exponentially (Eq. (5)), used for chip section:

$$D = \frac{L\bar{\epsilon}}{\bar{u}_f} = \frac{\bar{u}}{\bar{u}_f}; \quad (4)$$

$$D = 1 - \exp \left(- \int_0^{\bar{u}} \frac{\bar{\sigma}}{G_f} d\bar{u} \right). \quad (5)$$

Whereas, $\Delta \bar{\epsilon}$ is equivalent plastic strain increment and $\bar{\epsilon}_{0i}$ plastic strain at damage initiation. L is characteristic length assumed to the cubic root of the integration point element volume. G_f is fracture energy dissipation (required to open unit area of crack and is defined as a material parameter), \bar{u} is the equivalent plastic displacement and \bar{u}_f is the equivalent plastic displacement at failure expressed by following relation:

$$\bar{u}_f = \frac{2G_f}{\sigma_y}. \quad (6)$$

In ABAQUS[®], an element is deleted from the mesh if all of the section points at any one integration location have lost their load carrying capacity ($D = 1$). This is how the chip separation is realized from the workpiece. JC laws material entities and thermo-mechanical properties of the material used in the simulations are same as used in authors previous work [5]. These are specified in Table 1 and Table 2.

Table 1
Johnson-Cook material behaviour and damage parameters

A, MPa	B, MPa	n	C	m	D ₁	D ₂	D ₃	D ₄	D ₅
352	440	0.42	0.0083	1	0.13	0.13	-1.5	0.011	0

Table 2
Workpiece thermo-mechanical properties

Physical parameters	Workpiece (A2024-T351)
Density ρ , kg/m ³	2700
Young's modulus E , MPa	73000
Poisson's ratio ν	0.33
Fracture energy G_f , N/m	20E3
Specific heat C_p , Jkg ⁻¹ °C ⁻¹	0.557T+877.6
Expansion coefficient α_t , $\mu\text{m m}^{-1}$ °C	8.910 ⁻³ T+22.2
Thermal conductivity λ , W m ⁻¹ C ⁻¹	25 ≤ T ≤ 300: $\lambda = 0.247T + 114.4$ 300 ≤ T ≤ T _m : $\lambda = 0.125T + 226$
Melting temperature, T _m , °C	520
Room temperature, T _r , °C	25

3. Results

In the present section numerical results concerning 3D down cut milling process of an aluminium alloy A2024-T351 with the conceived 3D FE model (section 2) are discussed. Simulation results are presented in two

steps. Initially, the results with 3D model for $a_p \gg f$ (representing rough machining) are presented. The numerical results are compared with the experimental data in terms of chip morphology and cutting force. Subsequently, the results of the numerical investigations to study the effects of lower a_p values i.e. of the order of f (representing semi-finish and finish machining) in high speed machining regime (cutting speeds $V_C = 800$ and 1200 m/min) on surface finish and chip morphology are highlighted.

3.1. 3D numerical simulation for rough milling operation

Fig. 2 represents the chip morphology evolution for 3D down cut milling simulation, for cutting parameters: $a_p = 4$ mm, $f = 0.2$ mm/tooth, $V_C = 800$ m/min. It can be seen that, slightly segmented chip morphology (Fig. 2, a) is fairly comparable with the experimental one (Fig. 2, b). Big efforts are involved as UCT decreases in down cut milling case (with very fine mesh density), as already mentioned in section 2. Therefore, simulations were performed upto a radial depth of cut $a_e = 7.67$ mm, corresponding to $UCT = 160$ μ m. Break line on the experimental chip figures out a chip thickness variation from 200 μ m upto 160 μ m. Evolution of the cutting force for 3D down cut milling case is depicted in Fig. 3. Numerically registered cutting force is globally comparable with the experimental one, under investigated cutting conditions of tool geometry and cutting parameters [8].

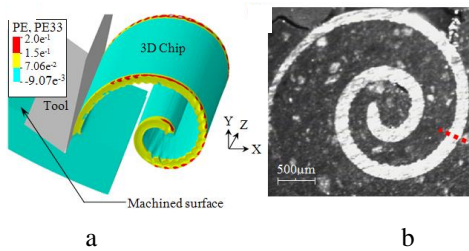


Fig. 2 Chip morphology for cutting parameters: $a_p = 4$ mm, $f = 0.2$ mm/tooth, $V_C = 800$ m/min a) simulated chip b) experimental chip

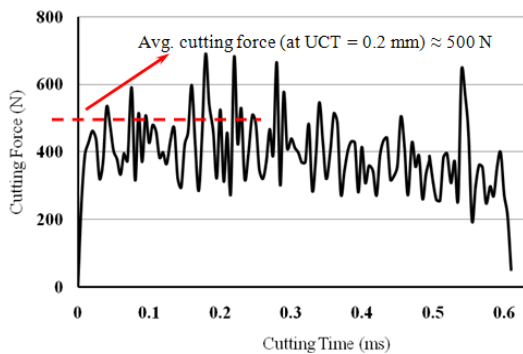


Fig. 3 Numerical cutting force for cutting parameters: $a_p = 4$ mm, $f = 0.2$ mm/tooth, $V_C = 800$ m/min

3.2. 3D numerical simulation for semi-finish and finish milling operations

Numerical results with the 3D model developed for rough machining, were found in reasonable correlation with the experimental ones. The model was then extended to semi-finish and finish machining cases. The global aim is to comprehend the multiphysical phenomena occurring

in the vicinity of tool chip interface during semi-finish and finish machining operations, which help to generate good surface finish (as compared to rough machining) in industrial high speed machining. Therefore, in the following the effects of the variation of a_p during high speed machining ($V_C = 800$ and 1200 m/min) on chip morphology and surface texture are discussed.

Fig. 4 represents numerical simulation result on spatial displacement of nodes along Z-axis, $U3$ (i.e. along depth of cut a_p) for cutting parameters: $a_p = 0.2$ mm, $f = 0.2$ mm/tooth, $V_C = 1200$ m/min. An average displacement of $U3 = 0.0862$ mm can be figured out. The percentage displacement of nodes along Z-axis ($U3, \%$) comes out 43.1.

Table 3 represents $U3$ and $\%U3$ when simulations were performed for other cutting parameters. It can be easily remarked that as a_p decreases $U3, \%$ increases. This consequently, results in higher plastic strains along Z-axis.

The numerically registered values of plastic strain component along Z-axis ($PE33$) for various cutting parameters are shown in Table 3.

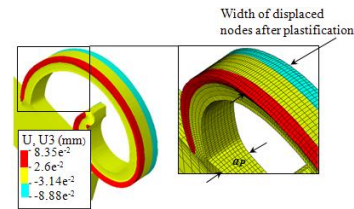


Fig. 4 Spatial displacement of nodes $U3$ (mm), for cutting parameters: $a_p = 0.2$ mm, $f = 0.2$ mm/tooth, $V_C = 1200$ m/min

Table 3 Numerical simulation results for $f = 0.2$ mm/tooth

V_C , m/min	Cutting operation	a_p , mm	Avg. $U3$, mm	$U3 = (U3 / a_p) \times 100, \%$	$PE33$
800	Rough	4	0.0713	1.78	0.2
	Semi-finish	1	0.0632	6.32	0.21
	Finish	0.2	0.0833	41.6	0.533
1200	Rough	4	0.0725	1.81	0.198
	Semi-finish	1	0.0676	6.76	0.232
	Finish	0.2	0.0862	43.1	0.584

Increasing values of $\%U3$ and $PE33$; as a_p decreases suggests that, an extended and larger $\%$ volume plasticises at lower a_p values. This results in an increase in material strength, because of the high requirement of inelastic dissipation of energy. This result is in consistence with recent research work of Liu and Melkote [9] on their study on material strengthening mechanisms and their contribution to size effect in micro cutting. They have shown in their 2D orthogonal machining numerical work that an edged radius tool widens the plasticisation zone in comparison to a sharp tool. This in turn requires higher energy dissipation, hence contributing to the size effect in micro cutting.

Frictional dissipation of energy, increases as cutting speed increases from 800 to 1200 m/min. This results in increasing the temperature leading to thermal softening. However, at these high cutting speeds strain rate hardening seems more dominant than the thermal softening phenomena, as can be deduced by the more regular and continuous chip morphology obtained at higher cutting speed (Fig. 5)

in comparison with the one obtained at lower cutting speed (Fig. 2). An increase in both %U3 and PE33 values can also be marked (Table 3) at higher cutting speed.

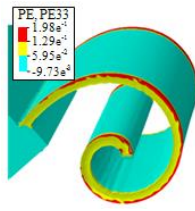


Fig. 5 Chip morphology for cutting parameters: $a_p = 4$ mm, $f = 0.2$ mm/tooth, $V_C = 1200$ m/min

An insight observation of Fig. 2-5 and Table 3 suggests that as a_p decreases and V_C increases, material strengthens by higher inelastic dissipation of energy and strain rate hardening phenomena. This generates a smooth continuous chip morphology (Fig. 4), if compared with one produced with higher a_p , and lower V_C values (Fig. 2). This in turn results in fine quality machined surface topology in high speed finishing operations, as shown in Fig. 6. This result is in good relation with findings of Mabrouki et al. [7]. They have shown in their numerical and experimental work on orthogonal machining that chip morphology dictates the quality of machined surface.

Figs. 6-8 represent the displacement of machined surface nodes along Z-axis for $a_p = 0.2$, 1 and 4 mm, respectively at two UCT and cutting speed values.

Generally, it can be seen that a decrease in a_p results in smoother machined surface textures. Conversely, numerical simulation results with high a_p depicts comparatively rough undulated surface texture.

It can also be observed in Figs. 6-8 that, as UCT decreases for down cut milling process surface quality improves. This can be attributed to the evolution of the chip morphology during milling operation. For example, in

Fig. 2 initially a segmented chip and onward at lower UCT a continuous (non segmented) chip morphology is obtained.

In this context, Nakayama and Tamura [10] believe that, as UCT reduces, shear plane angle becomes very small leading to greater plastic energy dissipations in the workpiece subsurface, thus strengthens the material.

While, Liu and Melkote [11] consider that a decrease in secondary deformation zone temperature contributes dominantly to strengthen the material as UCT decreases. Presence of high strain gradients at lower UCT also strengthens the material [5]. This shows that, multiple phenomena strengthen the material as UCT decreases, leading to continuous chip and smoother surface texture.

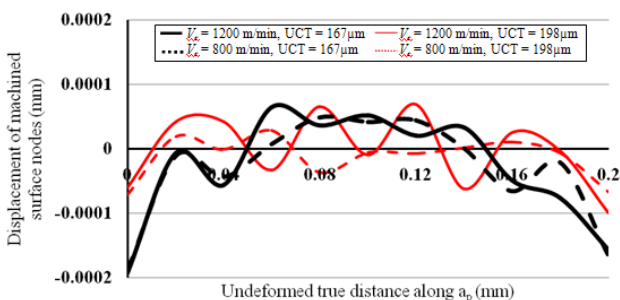


Fig. 6 Surface topology of machined surface along Z-axis for $a_p = 0.2$ mm

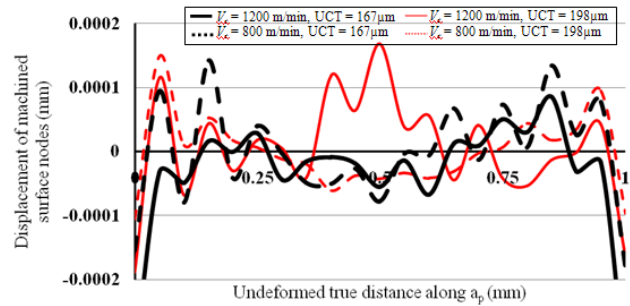


Fig. 7 Surface topology of machined surface along Z-axis for $a_p = 1$ mm

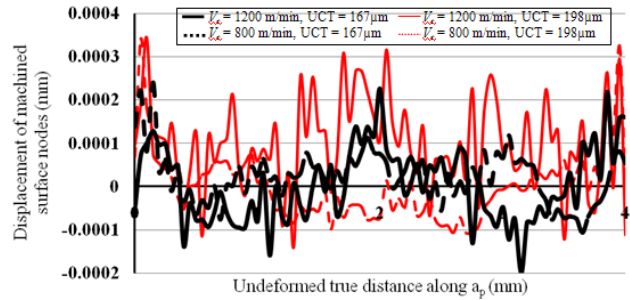


Fig. 8 Surface topology of machined surface along Z-axis for $a_p = 4$ mm

At high cutting speeds improved machined surfaces are obtained, as can be remarked in Figs. 6-8. This corresponds to smoother chips (non segmented) obtained at higher cutting speeds.

Finally, it can be stated that 3D cutting models are necessary for better comprehension of machining process, for instance for semi-finish and finish cutting operations, etc.

4. Conclusions

A 3D FE based numerical model for down cut milling process to investigate influence of cutting speed and depth of cut on chip morphology and surface finish has been developed. The prime objective is to bring comprehension of physical phenomena accompanying chip formation, which help to generate a smooth continuous (non segmented) chip morphology and better surface texture in semi-finish and finish cutting operations in high cutting speed regime.

Numerical simulation results show that the spatial displacement of nodes along Z-axis (along depth of cut) increases as depth of cut decreases (towards finish cutting). This eventually represents an extended and widened percentage of volume undergoing plastic deformation, resulting in higher dissipation of inelastic energy. The results also depict that material strain rate hardening characteristics increase the material strength at higher cutting speeds for the studied material. These strengthening phenomena help to generate a continuous chip and improved surface topology in high speed finishing operations.

Finally, the present study highlights only few of the many mutiphysical phenomena leading to high quality machined surface, during high speed semi-finish and finish machining operations. However, this contribution will allow an improvement in the existing cutting models and will help to optimize the cutting conditions. In future, ef-

fects of strain gradient hardening, tool geometries and machining conditions on 3D machined surface topology shall be focused.

References

1. **Asad, M.; Mabrouki, T.; Rigal, J.F.** 2010. Finite-element-based hybrid dynamic cutting model for aluminium alloy milling, *Proceedings of IMechE Part b: Journal of Engineering Manufacture* 224(1): 1-13. <http://dx.doi.org/10.1243/09544054JEM1590>.
2. **Tay, A.O.; Stevenson, M.G.; Davis, G.V.** 1974. Using the finite element method to determine temperature distributions in orthogonal machining, *Proceedings of IMechE* 188 (55): 627-638. http://dx.doi.org/10.1243/PIME_PROC_1974_188_074_02.
3. **Ceretti, E.; Lazzaroni, C.; Menegardo, L.; Altan, T.** 2000. Turning simulations using a three-dimensional FEM code, *Journal of Material Processing Technology* 98: 99-103. [http://dx.doi.org/10.1016/S0924-0136\(99\)00310-6](http://dx.doi.org/10.1016/S0924-0136(99)00310-6).
4. **Attanasio, A.; Ceretti, E.; Rizzuti, S.; Umbrello, D.; Micari, F.** 2008. 3D finite element analysis of tool wear in machining, *CIRP Annals Manufacturing Technology* 57: 61-64. <http://dx.doi.org/10.1016/j.cirp.2008.03.123>.
5. **Asad, M.; Mabrouki, T.; Girardin, F.; Zhang, Y.; Rigal, J.F.** 2011. Towards a physical comprehension of material strengthening factors during macro to micro scale milling, *Mechanika* 17(1): 97-104. <http://dx.doi.org/10.5755/j01.mech.17.1.210>.
6. **Asad, M.** 2010. Elaboration of concepts and methodologies to study peripheral down-cut milling process from macro-to-micro scales, PhD thesis, Insa Lyon France.
7. **Mabrouki, T.; Girardin, F.; Asad, M.; Rigal, J.F.** 2008. Numerical and experimental study of dry cutting for an aeronautic aluminium alloy (A2024-T351), *International Journal of Machine Tools and Manufacture* 48(11): 187-197.
8. **Zaghibani, I.; Songmene, V.** 2009. A force-temperature model including a constitutive law for dry high speed milling of aluminium alloys, *Journal of Material Processing Technology* 209(5): 2532-2544. <http://dx.doi.org/10.1016/j.jmatprotec.2008.05.050>.
9. **Liu, K.; Melkote, S.N.** 2007. Finite element analysis of the influence of tool edge radius on size effect in orthogonal micro-cutting process, *International Journal of Mechanical Science* 49(5): 650-660. <http://dx.doi.org/10.1016/j.ijmecsci.2006.09.012>.
10. **Nakayama, K.; Tamura, K.** 1968. Size effect in metal cutting force, *Journal of Engineering for Industry* 90(1): 119-126. <http://dx.doi.org/10.1115/1.3604585>.
11. **Liu, K.; Melkote, S.N.** 2006. Material strengthening mechanisms and their contribution to size effect in micro cutting, *Journal of Manufacturing Science and Engineering* 128(3): 730-738. <http://dx.doi.org/10.1115/1.2193548>.

M. Asad, T. Mabrouki

ALUMINIO LYDINIŲ FREZAVIMO PROCESO MODELIAVIMAS: 3D BEM TAIKYMAS

Re z i u m ė

Straipsnyje aprašomas 3D BEM taikymas pjovimo gylio ir pjovimo greičio įtakai paviršiaus ir drožlės morfologijai nustatyti apdirbant aliuminio lydinį A2024-T351. Pagrindinis tikslas – geriau suvokti drožlės susidarymo reiškinį pradedant paruošiamuoju ir baigiant glotniojo frezavimo pagal pastūmą procesu. Atlikta dviejų vienas po kito einančių žingsnių skaitinė analizė. Pirmiausia sukurta paruošiamąjo apdirbimo 3D modelis. Modeliavimo rezultatai palyginti su eksperimentiniais. Sukurti pusglotnio ir glotniojo apdirbimo skaitiniai modeliai. Nustatyta, kad atliekant glotniojo apdirbimo operacijas ruošinio mazginis perstūmimas išilgai pjovimo gylio būna didesnis. Tai reiškia, kad padidėja netamprios deformacijos tūrio procentas, taigi ir energijos sklaida. Be to, skaitmeniškai buvo nustatyta, kad, esant didesniems pjovimo greičiams, medžiaga sustiprėja dėl sukietinimo reiškinio veikiant tempimo deformacijoms. Šie sustiprinimo reiškiniai leidžia gauti ištisinę drožlę ir geros kokybės paviršiaus topologiją baigiamosiose pjovimo operacijose, atliekamose didesniais greičiais.

M. Asad, T. Mabrouki

ON THE MODELLING OF AN ALUMINIUM ALLOY MILLING: 3D FEM APPROACH

S u m m a r y

The present contribution put forwards a 3D FE approach to perform a parametric study on the effects of depth of cut and cutting speed on surface and chip morphologies, for machining an aerospace grade aluminium alloy A2024-T351. The ultimate objective is to improve the comprehension of chip formation phenomenon during rough to finish down cut milling process. Numerical investigations have been realized in two successive steps. Primarily, a 3D model for rough cut machining has been developed. Simulation results of later model were compared with the experimental ones. Onwards, numerical models for semi-finish to finish cutting cases were established. It was found that, workpiece nodal displacements along depth of cut are higher for finish cutting operations. This represents an increased percentage of volume under inelastic deformation, resulting in higher energy dissipation. Furthermore, it was numerically found that at higher cutting speeds material strengthens, due to strain rate hardening phenomenon. These strengthening phenomena results in continuous chips and fine quality surface topologies in finish cutting operations, performed at higher cutting speeds.

Keywords: milling modelling, FEM, Johnson-cook material model, A2024-T351.

Received July 09, 2012

Accepted October 10, 2013